Complex-valued sliding mode controllers for doubly-fed induction motors

Arnau Dòria-Cerezo, Md Abid Hossain, *Member, IEEE,* and Marc Bodson, *Fellow, IEEE,*

***Abstract*—This paper presents two algorithms to control the speed of doubly-fed induction motors. The controllers are designed using the complex-valued sliding mode methodology to track either the rotor or the stator current. An outer loop controls the mechanical speed. The control schemes are validated experimentally and compared on a laboratory setup.**

***Index Terms*—Complex-valued sliding mode control, Current control, Doubly-fed induction machines, Speed control**

I. Introduction

DOUBLY-fed induction machines (DFIM) are an attractive alternative in some applications due to their ability to be controlled through the rotor windings, and with power electronics that convert a fraction of the power required by conventional schemes. The use of DFIMs has been mainly related to variable speed generators, such as wind turbines [1] or flywheel energy storage systems [2]. However, the use of DFIMs for drive applications has also been considered for traction systems [3], marine applications [4], and aircraft propulsion [5].

The control of DFIMs has been studied in the literature using various methods. Most often, the schemes are based on reference frame orientation strategies such as the stator-flux oriented control [6], or the stator-voltage oriented control [7]. Other alternatives proposed to control DFIMs include nonlinear output feedback algorithms [8], passivity-based controllers [9], backstepping approaches [10], and robust controllers based on H_∞ optimization [11]. A different approach for the control of DFIMs is direct power control (DPC) [12], [13], or direct torque control (DTC) for drive applications. DPC is a table-based strategy with advantages of simplicity, low computational burden and fast dynamic responses. Compared to the methods mentioned above, DPC does not require a modulation component converting the continuous signals provided by the control algorithm into the switching signals.

Another family of controllers for DFIMs is the one based on sliding modes. Sliding mode controllers (SMC) applied to power converters exhibit the same characteristics as DPC: direct generation of on/off signals, simplicity of the control scheme, quick responses, together with robustness properties and tools to analyse the closed-loop stability [14]. However, the use of SMC for three-phase electrical machines still requires the Clarke and Park ($\alpha\beta$ or dq) transformations. This implies that the sliding manifolds defined by the control design do not correspond to the three-phase signals of the inverter, and the calculated switched control actions need to be converted.

Usually, the conversion from the dq coordinates to the three-phase switching signals is achieved by approximating the switched control actions obtained from the sliding mode algorithms by smooth functions and by a modulation stage through pulse-width modulation (PWM) or space-vector modulation (SVM). See examples in [15] [16], or a similar design using $\alpha\beta$-coordinates in [17]. Alternatively, the continuous control actions can be obtained using higher-order sliding modes, but still, the modulation stage is required. Examples include second-order sliding mode controllers [18] or the super-twisting algorithm [19]. Another approach to applying SMC in three-phase electrical machines is the use of a decoupling matrix that keeps the problem definition in the three-phase coordinates [20]. Still, the matrix strongly depends on the knowledge of the machine inductances, which are often affected by magnetic saturation.

The representation of induction machines using complex-valued dynamical models was proposed in [21] and was applied for the control of DFIMs [22]–[24]. The advantages of the complex-valued models are the order reduction and simplication of the control design. Recently, sliding modes techniques have been adapted to complex-valued systems [25] and applied to the control of squirrel-cage induction motors [26].

This paper aims to control a DFIM using complex-valued sliding modes. The benefits of using a complex-valued sliding mode controller (cSMC) are:

- Simple control algorithm
- Finite-time convergence
- No modulation stage required

The speed regulation of a DFIM is considered in this paper, using an internal loop based on cSMC for the machine currents. Two alternatives are presented: one controlling the rotor currents and another controlling the stator currents.

The paper is organized as follows. Section II presents the complex-valued model of the DFIM. The algorithm based on the control of the rotor currents is developed in Section III, and Section IV includes the stator current approach. The implementation procedure, regarding the generation of three-phase switching signals, is detailed in Section V. The results of the experimental validation are presented in Section VI. Finally, conclusions are stated in Section VII.

This work was supported in part by the Government of Spain through the *Agencia Estatal de Investigación* under Project PID2021-122821NB-I00.

A. Dòria-Cerezo is with the Dept. of Electrical Engineering and Inst. of Industrial and Control Engineering, Universitat Politècnica de Catalunya, Barcelona, Spain. arnau.doria@upc.edu.

M. A. Hossain and M. Bodson are with the Department of Electrical and Computer Engineering, The University of Utah, Salt Lake City, UT 84112, USA. mdabid.hossain@utah.edu; marc.bodson@utah.edu.

Notation

$j = \sqrt{-1}$ is used, instead of i, to avoid confusion with electrical currents; $\mathbb{C}^n$ denotes the complex n-dimensional space; for $z \in \mathbb{C}$, $\mathrm{Re}(z)$ and $\mathrm{Im}(z)$ denote the real and imaginary parts, respectively, z^*, $|z|$, and δ_z denote the conjugate, the magnitude, and the argument (angle), respectively.

II. DFIM MODEL

A. Three-phase to complex variables

Consider a three-phase electrical variable (voltage or current) given by $x_{abc}(t) = (x_a(t), x_b, (t), x_c(t))^T$. The transformation of $x_{abc} \in \mathbb{R}^3$ to a complex-valued variable, $z_{\alpha\beta} \in \mathbb{C}$ is defined by

$$z_{\alpha\beta}(t) = T x_{abc}(t) \tag{1}$$

where

$$T = c\left(1, e^{j\frac{2\pi}{3}}, e^{-j\frac{2\pi}{3}}\right), \tag{2}$$

for a constant c, with $c = \sqrt{\frac{2}{3}}$ preserving the definition of power (used in this paper), or $c = \frac{2}{3}$, maintaining the signal amplitude.

B. The DFIM complex model

A complex representation of the DFIM can be adapted from Chapter 2 of [27]. The dynamics of the DFIM after the complex transformation (1) is described by

$$L_s\frac{\mathrm{d}i_{s,\alpha\beta}}{\mathrm{d}t} + M\frac{\mathrm{d}}{\mathrm{d}t}\left(i_{r,\alpha\beta}e^{jn_p\theta}\right) = -R_s i_{s,\alpha\beta} + v_{s,\alpha\beta} \tag{3}$$

$$M\frac{\mathrm{d}}{\mathrm{d}t}\left(i_{s,\alpha\beta}e^{-jn_p\theta}\right) + L_r\frac{\mathrm{d}i_{r,\alpha\beta}}{\mathrm{d}t} = -R_r i_{r,\alpha\beta} + v_{r,\alpha\beta} \tag{4}$$

$$J\frac{\mathrm{d}\omega}{\mathrm{d}t} = -b\omega + \tau_e - \tau_L, \tag{5}$$

where $i_{s,\alpha\beta}, i_{r,\alpha\beta} \in \mathbb{C}$ are the stator and rotor currents; $v_{s,\alpha\beta} \in \mathbb{C}$ is the stator voltage; $v_{r,\alpha\beta} \in \mathbb{C}$ is the rotor voltage, which is used as a control input; $L_s, L_r, M \in \mathbb{R}$ are the stator, rotor and mutual inductances; $R_s, R_r \in \mathbb{R}$ are the stator and rotor resistances modelling the inductor losses; $J \in \mathbb{R}$ is the rotor inertia; $b \in \mathbb{R}$ is the damping coefficient; $n_p \in \mathbb{N}$ is the number of pole pairs; $\tau_L \in \mathbb{R}$ is the load torque, and $\tau_e \in \mathbb{R}$ is the electromagnetic torque given by

$$\tau_e = n_p M\ \mathrm{Im}(i_s\left(i_r e^{jn_p\theta}\right)^*). \tag{6}$$

C. The stator-voltage oriented complex model

The model of the DFIM in the stator-voltage oriented reference frame (also known as the dq-model) is obtained by defining the stator and rotor transformations

$$z_s = e^{-j\theta_e} z_{s,\alpha\beta} \tag{7}$$

$$z_r = e^{-j(\theta_e - n_p\theta)} z_{r,\alpha\beta}, \tag{8}$$

respectively. Complex variables $z_s, z_r \in \mathbb{C}$ refer to both voltages or currents, and the electrical phase $\theta_e(t)$, corresponds to argument of $v_{s,\alpha\beta}$. If $c = \sqrt{\frac{2}{3}}$ is used in (2), one gets

$$v_{s,\alpha\beta} = V_s e^{j\theta_e}, \tag{9}$$

where V_s is the magnitude of the complex voltage. V_s becomes the rms value of the stator line-to-line voltage in steady-state. However, complex variables are defined in arbitrary transient conditions as well. With the stator-voltage oriented model, $v_s = V_s e^{j0} = V_s \in \mathbb{R}$.

Using the transformations (7)-(8), the stator-voltage oriented model of a DFIM in the complex coordinates is

$$\begin{aligned} L_s\frac{\mathrm{d}i_s}{\mathrm{d}t} + M\frac{\mathrm{d}i_r}{\mathrm{d}t} =& -(R_s + j\omega_s L_s)i_s \\ & - j\omega_s M i_r + V_s \end{aligned} \tag{10}$$

$$\begin{aligned} M\frac{\mathrm{d}i_s}{\mathrm{d}t} + L_r\frac{\mathrm{d}i_r}{\mathrm{d}t} =& -j(\omega_s - n_p\omega)M i_s \\ & - \left(R_r + j(\omega_s - n_p\omega)L_r\right)i_r + v_r \end{aligned} \tag{11}$$

$$J\frac{\mathrm{d}\omega}{\mathrm{d}t} = -b\omega + \tau_e - \tau_L, \tag{12}$$

where $i_s, i_r \in \mathbb{C}$ are the stator-voltage oriented currents; $v_r \in \mathbb{C}$ is the rotor voltage (control input); $\omega_s \in \mathbb{R}$ is the stator frequency. In this new reference, the electromagnetic torque is given by

$$\tau_e = n_p M\ \mathrm{Im}(i_s i_r^*). \tag{13}$$

In steady-state, active and reactive powers, P and Q respectively, are equal to

$$P + jQ = V_s i_s^*. \tag{14}$$

D. Steady-state operation

The aim of a speed control algorithm for a DFIM is to follow the mechanical speed reference together with the regulation of the stator reactive power to a desired value, Q^d. Speed control can be achieved using a PI controller, where the control input is the commanded torque, τ_e^d. See details in the next section.

Combining the steady-state response of (10) with (13) and (14), the required stator current for given desired torque and reactive power, τ_e^d and Q^d, is

$$i_s^d = \frac{V_s}{2R_s} - \sqrt{\left(\frac{V_s}{2R_s}\right)^2 - \frac{\omega_s}{n_p R_s}\tau_e^d - \left(\frac{Q^d}{V_s}\right)^2} - j\frac{Q^d}{V_s}. \tag{15}$$

From the previous result, a limit is found to relate the attainable torque and reactive power, with

$$\left(\frac{V_s}{2R_s}\right)^2 \geq \frac{\omega_s}{n_p R_s}\tau_e^d + \left(\frac{Q^d}{V_s}\right)^2, \tag{16}$$

see more details in [24]. Assuming small rotor resistances, $R_s \approx 0$, the stator current becomes

$$i_s^d = \frac{\omega_s}{n_p V_s}\tau_e^d - j\frac{Q^d}{V_s}. \tag{17}$$

The corresponding desired rotor currents are obtained from the steady-state response of (11)

$$i_r^d = -\frac{L_s}{M}i_s^d - j\frac{1}{\omega_s M}\left(V_s - R_s i_s^d\right), \tag{18}$$

combined with (15). Neglecting the stator resistances and combining equation (18) with (17) results in

$$i_r^d = -\frac{L_s}{M}\frac{\omega_s}{n_p V_s}\tau_e^d - j\left(\frac{V_s}{\omega_s M} - \frac{L_s}{M}\frac{Q^d}{V_s}\right). \tag{19}$$

III. Speed controller based on a rotor current complex-valued SMC

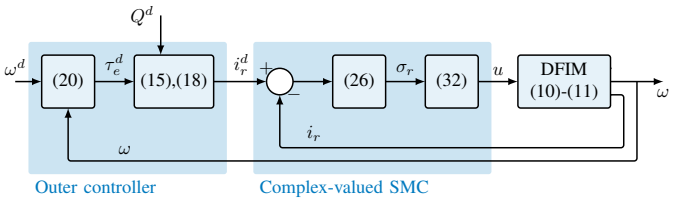

Fig. 1: Speed control scheme using the rotor currents (Rotor-cSMC).

The speed controller based on the rotor current feedback is shown in Figure 1. The outer speed control loop consists in a proportional-integral (PI) controller with the form

$$\tau_e^d = K_f K_p \omega^d - K_p \omega + K_i \int (\omega^d - \omega) \mathrm{d}\tau, \tag{20}$$

where K_p, K_i are the PI gains, and K_f is a feedforward gain applied to shift the location of the closed-loop zero and avoid an overshoot in the speed response. Letting $K_p = 2a_v J$ and $K_i = a_v^2 J$, where J is the moment of inertia of the motor and load, the closed-loop poles of the velocity loop are placed at $s = -a_v$. The value $K_f = 2/3$ yields a fast response without overshoot. See more details in [24]. The required rotor current is calculated from (19) with the torque command obtained in (20) and the desired reactive power Q^d.

The inner current loop based on complex-valued sliding modes (called Rotor-cSMC), ensuring that i_r reaches i_r^d in finite time, is described below.

A. Complex-valued sliding mode rotor current controller

The complex-valued algorithm is based on a switching action in the complex plane that is equivalent to switching between values described by a circumference, see details in [25]. Since $c = \sqrt{\frac{2}{3}}$ is used in (2), the admissible rotor voltages are described by

$$v_r = V_{dc} u, \tag{21}$$

where $u \in \mathbb{C}$ has unity modulus, $V_{dc} = 2\sqrt{2/3}\, v_{dc}$, if the DC voltage of the three-phase inverter used to generate the rotor voltages is defined between $\pm v_{dc}$.

Using (21), the electrical equations in (10) and (11) can be written as

$$\mu \frac{\mathrm{d}i_s}{\mathrm{d}t} = \Phi_s - M V_{dc} u \tag{22}$$

$$\mu \frac{\mathrm{d}i_r}{\mathrm{d}t} = \Phi_r + L_s V_{dc} u \tag{23}$$

where $\mu = L_s L_r - M^2 > 0$, and

$$\begin{aligned}\Phi_s =& -(L_r R_s + j\omega_s \mu + j n_p \omega M^2) i_s \\ &+ (R_r - j n_p \omega L_r) M i_r + L_r V_s \end{aligned} \tag{24}$$

$$\begin{aligned}\Phi_r =& (R_s + j n_p \omega L_s) M i_s \\ &- (R_r L_s + j\omega_s \mu - j n_p \omega L_r L_s) i_r - M V_s. \end{aligned} \tag{25}$$

The sliding manifold proposed to track the rotor current reference, i_r^d, is

$$\sigma_r = i_r - i_r^d. \tag{26}$$

The equivalent control is defined such that $\dot{\sigma}_r = 0$. Differentiating (26) with respect to time and using (23), one gets

$$\dot{\sigma}_r = \frac{1}{\mu}\Phi_r + \frac{L_s}{\mu} V_{dc} u - \frac{\mathrm{d}i_r^d}{\mathrm{d}t}, \tag{27}$$

so that the equivalent control is given by

$$u_{\text{eq}} = -\frac{1}{V_{dc} L_s}\Phi_r + \frac{\mu}{V_{dc} L_s}\frac{\mathrm{d}i_r^d}{\mathrm{d}t}. \tag{28}$$

Consider the Lyapunov function candidate

$$W_r = \frac{1}{2}\sigma_r^* \sigma_r. \tag{29}$$

The time derivative of (29) can be written as

$$\begin{aligned}\dot{W}_r &= \frac{1}{2}\left(\dot{\sigma}_r^* \sigma_r + \sigma_r^* \dot{\sigma}_r\right) \\ &= \mathrm{Re}\left(\sigma_r^* \dot{\sigma}_r\right) \\ &= \mathrm{Re}\left(\sigma_r^* \left(\frac{1}{\mu}\Phi_r + \frac{L_s}{\mu} V_{dc} u - \frac{\mathrm{d}i_r^d}{\mathrm{d}t}\right)\right). \end{aligned} \tag{30}$$

Using the equivalent control definition

$$\dot{W}_r = \mathrm{Re}\left(\sigma_r^* \frac{L_s}{\mu} V_{dc}\left(u - u_{\text{eq}}\right)\right), \tag{31}$$

and the switching control policy

$$u = -\frac{\sigma_r}{|\sigma_r|}, \tag{32}$$

one gets

$$\begin{aligned}\dot{W}_r &= \mathrm{Re}\left(\sigma_r^* \frac{L_s}{\mu} V_{dc}\left(u - u_{\text{eq}}\right)\right) \\ &= -V_{dc}\frac{L_s}{\mu}\mathrm{Re}\left(\sigma_r^*\left(\frac{\sigma_r}{|\sigma_r|} + u_{\text{eq}}\right)\right) \\ &= -V_{dc}\frac{L_s}{\mu}\mathrm{Re}\left(|\sigma_r| + \sigma_r^* u_{\text{eq}}\right) \\ &= -V_{dc}\frac{L_s}{\mu}|\sigma_r|\mathrm{Re}\left(1 + \frac{\sigma_r^*}{|\sigma_r|}u_{\text{eq}}\right) \\ &= -V_{dc}\frac{L_s}{\mu}|\sigma_r|\mathrm{Re}\left(1 + |u_{\text{eq}}| e^{j(\delta_{\text{eq}} - \delta_{\sigma_r})}\right) \\ &= -V_{dc}\frac{L_s}{\mu}|\sigma_r|\left(1 + |u_{\text{eq}}|\cos(\delta_{\text{eq}} - \delta_{\sigma_r})\right). \end{aligned} \tag{33}$$

The sliding motion. $\dot{W}_r < 0$, is guaranteed if

$$|u_{\text{eq}}| < 1. \tag{34}$$

Remark 1: As expected, the control action must remain within the circle of unity radius. Note also that u_{eq} can be reduced by increasing the inverter dc voltage.

B. Ideal sliding dynamics

The ideal dynamics occur when $\dot{\sigma}_r = \sigma_r = 0$ and describe how the system behaves during the sliding motion. From (22), replacing u by the equivalent control obtained in (28)

$$\mu \frac{\mathrm{d}i_s}{\mathrm{d}t} = \Phi_s + \frac{M}{L_s}\Phi_r - \mu\frac{M}{L_s}\frac{\mathrm{d}i_r^d}{\mathrm{d}t}. \tag{35}$$

Further, using (24)-(25),

$$\frac{\mathrm{d}i_s}{\mathrm{d}t} = -(R_s + j\omega_s L_s) i_s + v_s - M\left(j\omega_s i_r^d - \frac{\mathrm{d}i_r^d}{\mathrm{d}t}\right), \tag{36}$$

which is stable since $R_s > 0$.

IV. Speed Controller Based on a Stator Current Complex-Valued SMC

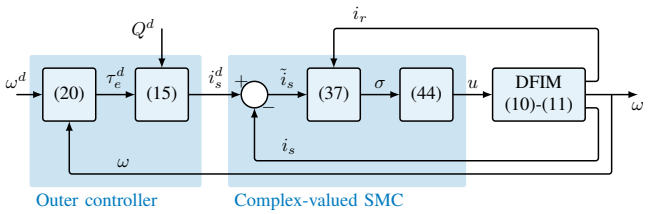

Fig. 2: Speed control scheme using the stator currents (Stator-cSMC).

Figure 2 shows the control scheme based on a stator current control (Stator-cSMC). The outer loop is the same as in Section III, but using the stator current reference equation (17) instead of (19). The cSMC required to track the stator current reference is different. Details are given in the next sections.

A. Complex-valued sliding mode stator current controller

The proposed sliding manifold is

$$\sigma_s = k_p\tilde{i}_s + k_i\int \tilde{i}_s \mathrm{d}\tau - i_r, \tag{37}$$

where $k_p, k_i \in \mathbb{C}$, and

$$\tilde{i}_s = i_s - i_s^d. \tag{38}$$

This PI-like structure of the switching manifold is justified in the analysis of the ideal sliding dynamics and further discussed in Section IV-C.

Differentiating (37) with respect to time, using (22)-(23), and after some algebra,

$$\dot{\sigma}_s = \frac{k_p}{\mu}\Phi_s - \frac{1}{\mu}\Phi_r + k_i\tilde{i}_s - k_p\frac{\mathrm{d}i_s^d}{\mathrm{d}t} - \frac{\kappa}{\mu}V_{dc}u, \tag{39}$$

where

$$\kappa = k_pM + L_s. \tag{40}$$

κ is a complex parameter that can be tuned using k_p. From (39), the equivalent control is defined as

$$u_{\text{eq}} = \frac{1}{V_{dc}\kappa}\left(k_p\Phi_s - \Phi_r + k_i\mu\tilde{i}_s - k_p\mu\frac{\mathrm{d}i_s^d}{\mathrm{d}t}\right). \tag{41}$$

Similarly to Section III, consider the Lyapunov function candidate

$$W_s = \frac{1}{2}\sigma_s^*\sigma_s, \tag{42}$$

whose time derivative is

$$\dot{W}_s = -\mathrm{Re}\left(\sigma_s^*\frac{V_{dc}}{\mu}\kappa\left(u - u_{\text{eq}}\right)\right). \tag{43}$$

Then, with the switching control policy

$$u = \frac{\sigma_s}{|\sigma_s|}, \tag{44}$$

one gets

$$\dot{W}_s = -\cos(\delta_\kappa)V_{dc}\frac{|\kappa|}{\mu}|\sigma_s|\left(1 - |u_{\text{eq}}|\cos(\delta_\sigma - \delta_{\text{eq}})\right). \tag{45}$$

The sliding motion is guaranteed if

$$\cos(\delta_\kappa) > 0 \tag{46}$$

$$|u_{\text{eq}}| < 1. \tag{47}$$

The result suggests using k_p such that $\delta_\kappa \in \left(-\frac{\pi}{2}, \frac{\pi}{2}\right)$, for example $k_p \in \mathbb{R}$ and positive.

B. Ideal sliding dynamics and control tuning

The ideal sliding dynamics with the stator current controller are different from those obtained in Section III-B. From (23), replacing u by the equivalent control obtained in (41) and after some algebra

$$\begin{aligned}\kappa\frac{\mathrm{d}i_r}{\mathrm{d}t} =& -k_p(R_s + j\omega_sL_s)i_s - jk_p\omega_sMi_r \\ &+ k_iL_s\tilde{i}_s - k_pL_s\frac{\mathrm{d}i_s^d}{\mathrm{d}t} + k_pV_s.\end{aligned} \tag{48}$$

On the other hand, from (37) with $\dot{\sigma}_s = 0$, one gets

$$k_p\frac{\mathrm{d}\tilde{i}_s}{\mathrm{d}t} + k_i\tilde{i}_s - \frac{\mathrm{d}i_r}{\mathrm{d}t} = 0. \tag{49}$$

Combining (48) with (49) results in the complex-valued linear dynamics

$$\begin{aligned}\kappa\frac{\mathrm{d}i_r}{\mathrm{d}t} =& -k_p(R_s + j\omega_sL_s)i_s - jk_p\omega_sMi_r + k_iL_s\tilde{i}_s \\ &+ k_pV_s - k_pL_s\frac{\mathrm{d}i_s^d}{\mathrm{d}t}\end{aligned} \tag{50}$$

$$\begin{aligned}\kappa\frac{\mathrm{d}\tilde{i}_s}{\mathrm{d}t} =& -(R_s + j\omega_sL_s)i_s - j\omega_sMi_r + V_s \\ &- k_iM\tilde{i}_s - L_s\frac{\mathrm{d}i_s^d}{\mathrm{d}t}\end{aligned} \tag{51}$$

The state matrix of (50)-(51) is

$$A_{CL} = \frac{1}{\kappa}\begin{pmatrix} -jk_p\omega_sM & -k_p(R_s + j\omega_sL_s) + k_iL_s \\ -j\omega_sM & -(R_s + j\omega_sL_s) - k_iM \end{pmatrix} \tag{52}$$

with a characteristic polynomial,

$$\det(sI - A_{CL}) = s^2 + (a_1 + jb_1)s + (a_2 + jb_2), \tag{53}$$

where

$$a_1 = \frac{R_s + k_iM}{\kappa} \tag{54}$$

$$b_1 = \omega_s \tag{55}$$

$$a_2 = 0 \tag{56}$$

$$b_2 = \frac{k_i\omega_sM}{\kappa}. \tag{57}$$

Using the Complex Hurwitz test [22], stability is guaranteed if coefficients of (53) satisfy

$$a_1 > 0 \tag{58}$$

$$\begin{vmatrix} a_1 & 0 & -b_2 \\ 1 & a_2 & -b_1 \\ 0 & b_2 & a_1 \end{vmatrix} > 0. \tag{59}$$

Assuming $R_s, \omega_s, \kappa > 0$, the conditions simplify to

$$R_s + k_iM > 0. \tag{60}$$

Tuning the controller consists in finding the values of k_p, k_i fulfilling the conditions (46), (47) and (60). Note that (46) and (60) are automatically satisfied if the gains are real and positive.

C. Why a "direct" current stator approach is not adequate?

In this section, it is shown that the simpler choice

$$\sigma_s = \tilde{i}_s \tag{61}$$

fails to ensure stability and the proposed sliding manifold in (37).

Differentiating (61) with respect to time gives

$$\dot{\sigma}_s = \frac{1}{\mu}\left(\Phi_s - MV_{dc}u\right) - \frac{\mathrm{d}i_s^d}{\mathrm{d}t} \tag{62}$$

and the equivalent control is

$$u_{eq} = \frac{1}{MV_{dc}}\left(\Phi_s - \mu\frac{\mathrm{d}i_s^d}{\mathrm{d}t}\right). \tag{63}$$

Now, assuming that the sliding motion is guaranteed, $\sigma_s = 0$, and replacing $u = u_{\text{eq}}$, $i_s = i_s^d$ in (23), the rotor current dynamics results in

$$\frac{\mathrm{d}i_r}{\mathrm{d}t} = -j\omega_s i_r + \frac{1}{M}V_s - \frac{1}{M}(R_s + j\omega_s L_s)i_s^d - \frac{L_s}{M}\frac{\mathrm{d}i_s^d}{\mathrm{d}t}. \tag{64}$$

The rotor dynamics in (64) are only marginally stable. This result confirms the dynamic analysis of the direct stator current approaches presented in [28].

V. Control Law Implementation

The control designs proposed in the previous sections are based on the stator-voltage oriented frame and, in a practical scenario, need to be embedded in an overall control scheme containing the three-phase to complex transformations, and vice-versa. Figure 3 shows the block diagram of the controller with all the necessary transformations. Equations (1), (7) and (8) are used to calculate the complex currents and voltages from three-phase variables, which are then used in the complex sliding mode controller. The complex control action in the $\alpha\beta$ complex framework is obtained from (8) as

$$u_{\alpha\beta} = e^{j(\theta_e - n_p\theta)}u. \tag{65}$$

The three-phase switching signals, s_{abc}, are obtained from $u_{\alpha\beta}$ as described in the next subsection.

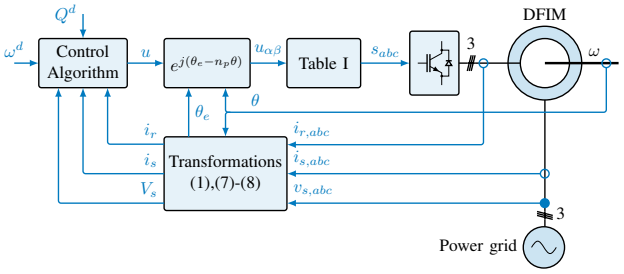

Fig. 3: Overall control scheme.

A. From complex to three-phase switching signals

Using (65), the control signal is

$$u_{\alpha\beta} = e^{j(\theta_e - n_p\theta)}\frac{\sigma}{|\sigma|}. \tag{66}$$

which results in

$$u_{\alpha\beta} = e^{j(\theta_e - n_p\theta + \delta_\sigma)}. \tag{67}$$

The control values are restricted to the unit circle in the complex plane (see the blue circle in Figure 4). Additionally, the use of a switching converter limits the available control values to a finite set defined by applying the transformation (1) to the vector

$$s_w = (s_a, s_b, s_c)^T \tag{68}$$

where, for a two-level bridge converter, $s_i = \{-1, 1\}$ for $i = a, b, c$. Black dots in Figure 4 correspond to the admissible values for a two-level bridge converter.

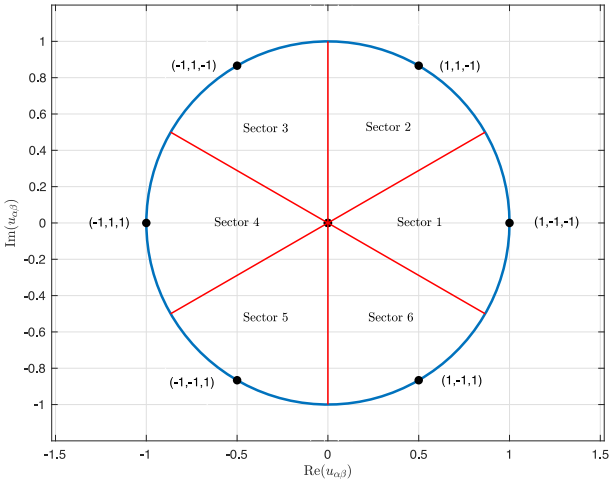

Fig. 4: Complex control values from (44) with a unit magnitude, blue circle. Black dots correspond to the admissible values for a two-level bridge converter.

The rationale of the switching policy is to approximate the control value on the blue circle to the closer available switch combination. This procedure divides the complex plane into six sectors, as shown in Figure 4. In other words, this strategy assigns a sector from the angle of $u_{\alpha\beta}$, and the switching policy is obtained form Table I.

$\angle u_{\alpha\beta}$	Sector	s_a	s_b	s_c
$-30° \to 30°$	1	1	-1	-1
$30° \to 90°$	2	1	1	-1
$90° \to 150°$	3	-1	1	-1
$150° \to 210°$	4	-1	1	1
$210° \to 270°$	5	-1	-1	1
$270° \to 330°$	6	1	-1	1

TABLE I: From complex control values to three-phase abc switching values for a 2-level converter.

VI. Experimental Results

Figure 5 shows the experimental setup. In the figure, GS stands for grid supply, CS for current sensor, VS for voltage sensor, and IM for induction motor (a squirrel-cage induction

machine was used as a load). Simulink programs are loaded on the dSPACE DS1104 module, which works as the interface for data acquisition and control. The grid supply is at 60 Hz and is stepped down from 120 V (phase rms) to approximately 7.6 V by the transformer box. The relay box can connect or disconnect the lower voltage grid supply to/from the stator windings of the DFIM. The relay control signal comes through the dSPACE module from a user interface. The relay box also includes a voltage reduction network for voltage measurement. The oscilloscope captures four signals, two phases (A and B) each of the stator voltages and the grid voltages from the relay box to check the magnitudes, phase sequences, and phase angles. A current sensor measures the current that flows into the DFIM stator from the grid. The induction machine, mechanically coupled with the DFIM, sends the position data to dSPACE. This induction machine enables the option of applying a variable load using a separate electrical supply (not shown in Figure 5). The Hirel board, controlled by dSPACE, supplies power to the rotor windings of the DFIM and sends the current measurements to dSPACE. Table II shows the values of the DFIM parameters.

According to [24], the code computes torque limits in real-time. The computation ensures that the rotor currents stay within a bound $i_{r,\max}$, in coordination with an anti-windup procedure in the PI velocity controller in (20). Table III shows the values of the controller parameters. The PI gains of the current loop for the Stator-cSMC scheme place the poles of (53) at $s_1 = -27.7 - j365.8$ and $s_2 = -148.1 - j11.2$. For k_i large, it turns out that one of the roots of (53) moves towards $s = -j\omega_s$, while the other root is approximately given by $s = -k_i M/\kappa$ (with the values given, the estimate of the second pole is $s = -144.5$, which is close to s_2). The underdamped pole s_1 could cause concern, but this pole is largely cancelled by a zero of the system at $s = -j\omega_s$. The zero is due to the impossibility of inducing a DC current on the stator using the rotor currents.

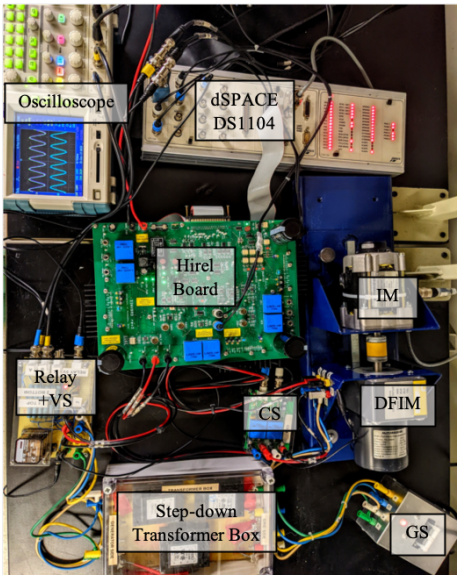

Fig. 5: Setup of the experimental testbed.

Symbols	Parameters	Values
R_s	DFIM stator resistance	0.66 Ω
R_r	DFIM rotor resistance	0.94 Ω
L_s	DFIM stator inductance	13.1 mH
L_r	DFIM rotor inductance	9.8 mH
M	DFIM mutual inductance	9.7 mH
n_p	DFIM number of pole pairs	2
J	Total moment of inertia	3.5×10^{-4} kg m^2

TABLE II: List and values of the machine parameters.

Symbols	Parameters	Values
a_v	Desired pole for the speed loop	31.4 rad/s
k_p	Proportional gain (Stator-cSMC)	0.82
k_i	Integral gain (Stator-cSMC)	314
$i_{r,\max}$	Maximum rotor current (peak, per phase)	6 A
v_{dc}	Maximum rotor voltage (peak, per phase)	7 V
f_s	Sampling frequency	5 kHz

TABLE III: List and values of the control parameters.

The first test consists of a reference profile from standstill to 1800 rpm and changes of 30% above and below (see speed profile in Figure 6). The desired stator reactive power is set to zero and is not regulated with a feedback loop. Normally, a separate procedure would be used to start the motor, but it was decided to use the same controller with a brief increase in rotor voltage, so that the capabilities of the control law could be evaluated with a large transient command.

Figures from 6 to 9 compare the results obtained using the two controllers proposed in Sections III and IV. The speed behavior is almost identical because of the successful current regulation of the inner loops and the common speed controller, see Figure 6. The stator active and reactive powers are plotted in Figure 7. The schemes were not designed to precisely track the zero reactive power command, but tracking is found to be superior with the stator current controller (bottom plot in Figure 7). The error in the reactive power is associated with the open-loop nature of this part of the control system and the uncertainties in the parameters used to calculate (18).

Figures 8 and 9 show the real and imaginary parts of the complex rotor and stator currents when using the Rotor-cSMC and Stator-cSMC, respectively. One may observe that the real and imaginary components of the currents are biased relative to their references. This effect can be explained in two ways. First, the control implementation is in discrete-time with application to a nonlinear system. Biases are known to occur in such cases even for real-valued sliding modes. Second, the proposed method works in the complex domain and treats the current components as a whole (the switching policy does not depend separately on the real and imaginary components). This effect becomes more noticeable when using the Rotor-cSMC around zero speed, in the first and last seconds in Figure 8.

The second test consists in a sudden pulse of load torque. An external load, approximately 0.12 N m in magnitude, is applied at approximately $t = 0.5$ s for 0.5 s. Figures from 10 to 13 compare the results when using the Rotor-cSMC and the Stator-cSMC. Again, the mechanical speed is similar for the two algorithms (Figure 10), and the Stator-cSMC performs better in regulating the reactive power (Figure 11) and the currents (Figures 12 and 13).

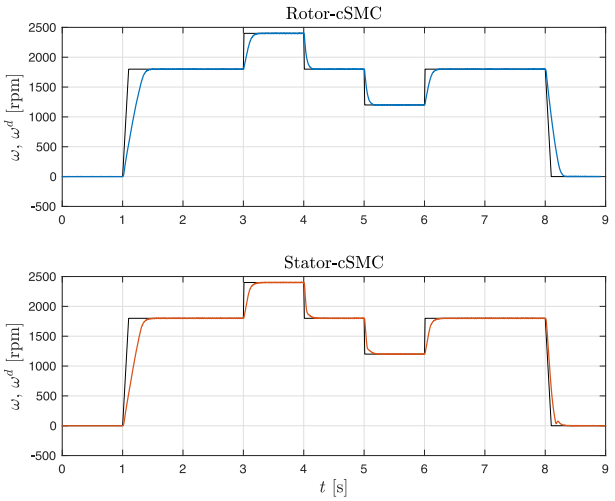

Fig. 6: Experimental results (Test 1, speed reference change): Mechanical speed using the rotor current controller (top) and the stator current controller (bottom). Reference speed black line.

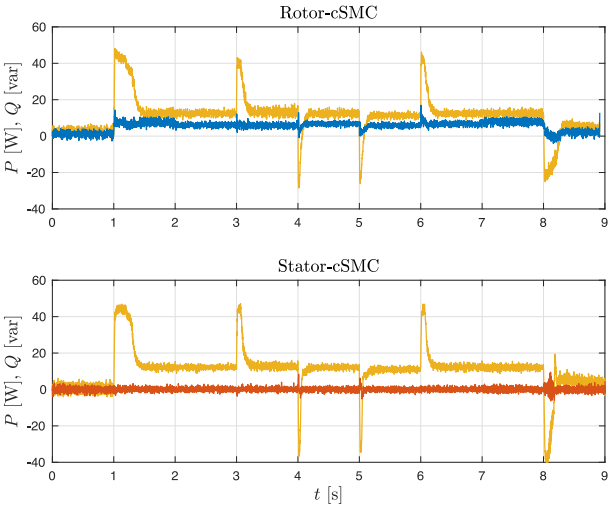

Fig. 7: Experimental results (Test 1, speed reference change): Active and reactive powers (P and Q) using the rotor current controller (top) and the stator current controller (bottom). Active power, P, in yellow, and reactive power, Q, in blue (top) or red (bottom).

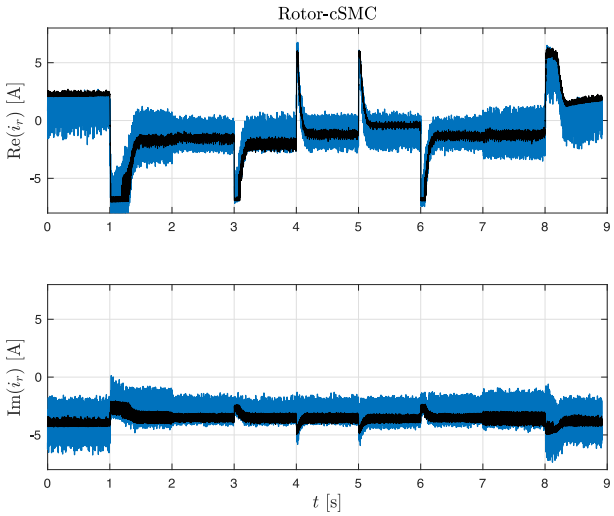

Fig. 8: Experimental results (Test 1, speed reference change): Real and imaginary parts of the rotor current, top and bottom, respectively, when using the Rotor-cSMC. Reference current provided by the PI controller and equations (15) and (18) in black line.

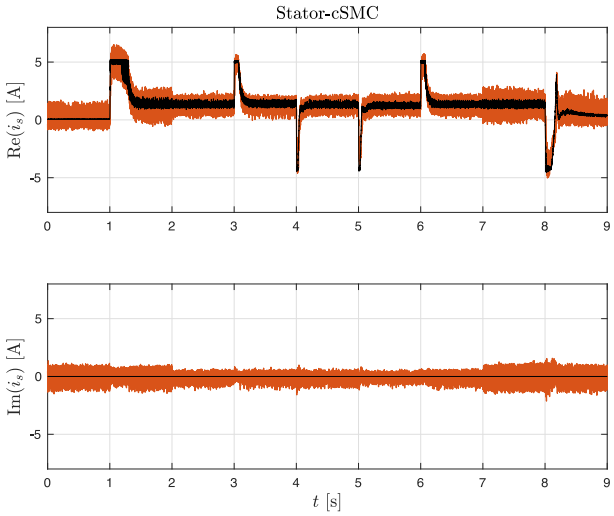

Fig. 9: Experimental results (Test 1, speed reference change): Real and imaginary parts of the stator current, top and bottom respectively, when using the Stator-cSMC. Reference current provided by the PI controller and equation (15) in black line.

VII. Conclusions

This paper proposed two control schemes for the speed regulation of a DFIM based on complex-valued sliding modes. In the experimental tests, the Stator-cSMC algorithm performed better than the Rotor-cSMC. The error in the reactive power may not be important for motor operation but, if necessary, an outer loop for the reactive power could be added to reduce the effect of parameter uncertainties. Given the simplicity of the Rotor-cSMC, a dedicated controller could be implemented at a higher sampling rate than those feasible in the test setup, and would likely result in improved current tracking performance.

Compared to control methods such as PI controllers, the advantages of the proposed method are i) simplicity, ii) absence of a modulation stage (for example, PWM) with direct control of switches, iii) no command limiting of rotor voltages needed, and, for the Rotor-cSMC, iv) no parameter needed, as opposed to impedances used for the coupling terms in standard PI controllers. Disadvantages of cSMC algorithms are: i) higher current fluctuations at the same sampling time, and ii) offset in filtered currents (more noticeable for the rotor control algorithm).

References

[1] M. G. Simoes and F. A. Farret, *Renewable Energy Systems: Design and Analysis with Induction Generators*. CRC Press, 2004.

[2] H. Akagi and H. Sato, "Control and performance of a doubly-fed induction machine intended for a flywheel energy storage system," *IEEE Trans. on Power Electronics*, vol. 17, no. 1, pp. 109–116, 2002.

[3] R. S. Muñoz-Aguilar, A. Dòria-Cerezo, and P. F. Puleston, "Direct synchronous-asynchronous conversion system for hybrid electrical vehicle applications. an energy-based modeling approach," *International Journal of Electrical Power & Energy Systems*, vol. 47, pp. 264–279, 2013.

[4] M. Debbou, A. Damdoum, and M. P. David, "Optimal sliding mode control for DFIM electric marine thruster," in *Proc. International*

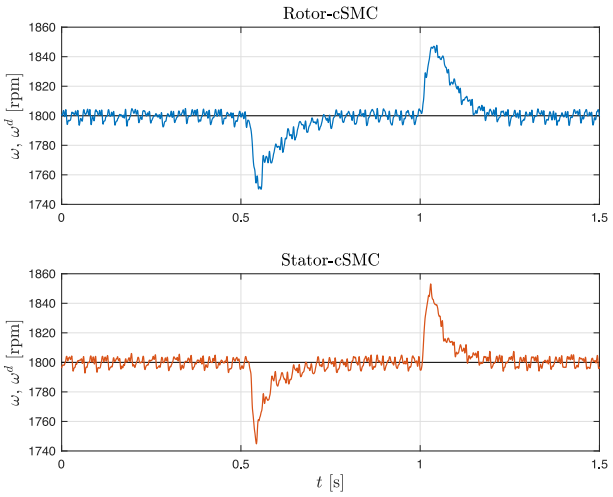

Fig. 10: Experimental results (Test 2, pulse of load torque): Mechanical speed using the rotor current controller (top) and the stator current controller (bottom). Reference speed black line.

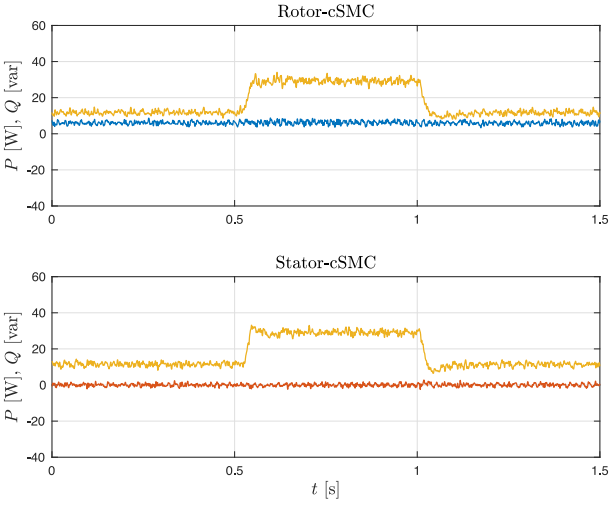

Fig. 11: Experimental results (Test 2, pulse of load torque): Active and reactive powers (P and Q) using the rotor current controller (top) and the stator current controller (bottom). Active power, P, in yellow, and reactive power, Q, in blue (top) or red (bottom).

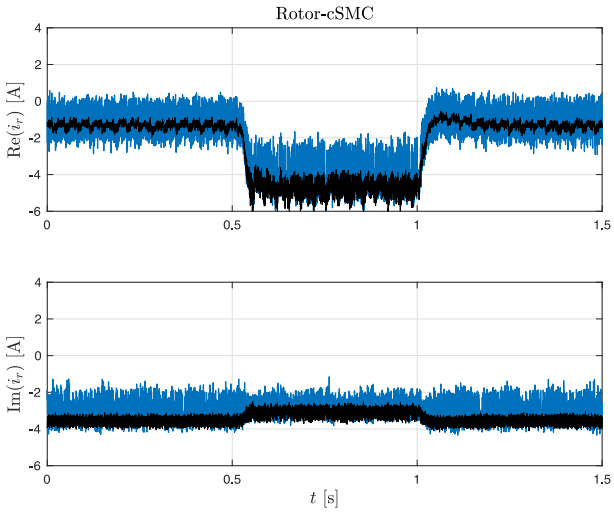

Fig. 12: Experimental results (Test 2, pulse of load torque): Real and imaginary parts of the rotor current, top and bottom respectively, when using the Rotor-cSMC. Reference current provided by the PI controller and equations (15) and (18) in black line.

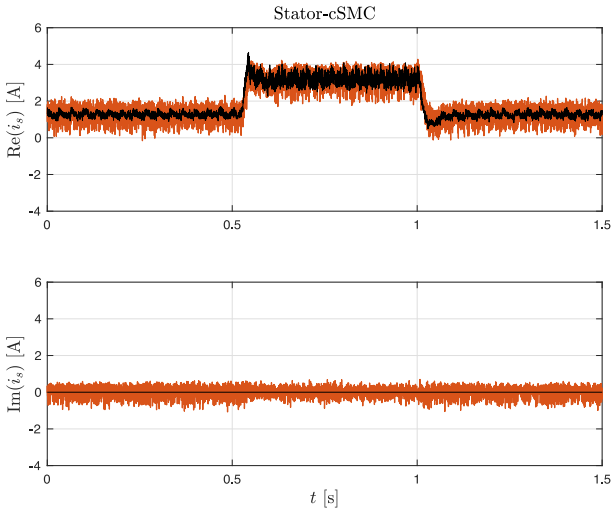

Fig. 13: Experimental results (Test 2, pulse load torque): Real and imaginary parts of the stator current, top and bottom respectively, when using the Stator-cSMC. Reference current provided by the PI controller and equation (15) in black line.

Conference on Electrical Systems for Aircraft, Railway, Ship Propulsion and Road Vehicles & International Transportation Electrification Conference, 2016.

[5] D. J. Sadey, L. Taylor, and R. Beach, "Proposal and development of a high voltage variable frequency alternating current power system for hybrid electric aircraft," in *Proc. 14th International Energy Conversion Engineering Conference*, 2016.

[6] R. Peña, J. C. Clare, and G. M. Asher, "Doubly fed induction generator using back-to-back PWM converter and is application to variable-speed wind–energy generation," *IEE Proceedings - Electric Power Applications*, vol. 143, no. 3, pp. 231–241, 1996.

[7] S. Muller, M. Deicke, and R. W. D. Doncker, "Doubly fed induction generator systems for wind turbines," *IEEE Industry Applications Magazine*, vol. 8, no. 3, pp. 26–33, 2002.

[8] S. Peresada, A. Tilli, and A. Tonielli, "Indirect stator flux-oriented output feedback control of a doubly fed induction machine," *IEEE Trans. on Control Systems Technology*, vol. 11, no. 6, pp. 875–888, 2003.

[9] C. Batlle, A. Dòria-Cerezo, and R. Ortega, "Power flow control of a doubly-fed induction machine coupled to a flywheel," *European Journal of Control*, vol. 11, no. 3, pp. 209–221, 2005.

[10] A. Gensior, T. M. P. Nguyen, J. Rudolph, and H. Güldner, "Flatness-based loss optimization and control of a doubly fed induction generator system," *IEEE Trans. on Control Systems Technology*, vol. 19, no. 6, pp. 1457–1466, 2011.

[11] B. Qin, H. Sun, J. Ma, W. Li, T. Ding, Z. Wang, and A. Y. Zomaya, "Robust H_∞ control of doubly fed wind generator via state-dependent Riccati equation technique," *IEEE Trans. on Power Systems*, vol. 34, no. 3, pp. 2390–2400, 2019.

[12] Y. Zhang, J. Jiao, and D. Xu, "Direct power control of doubly fed induction generator using extended power theory under unbalanced network," *IEEE Trans. on Power Electronics*, vol. 34, no. 12, pp. 12 024–12 037, 2019.

[13] S. Gao, H. Zhao, Y. Gui, D. Zhou, and F. Blaabjerg, "An improved direct power control for doubly fed induction generator," *IEEE Trans. on Power Electronics*, vol. 36, no. 4, pp. 4672–4685, 2021.

[14] V. Utkin, J. Guldner, and J. Shi, *Sliding Mode Control in Electro-Mechanical Systems*. CRC Press, 1999.

[15] L. Shang and J. Hu, "Sliding-mode-based direct power control of grid-connected wind-turbine-driven doubly fed induction generators under unbalanced grid voltage conditions," *IEEE Trans. on Energy Conversion*, vol. 27, no. 2, pp. 362–373, 2012.

[16] L. Xiong, J. Wang, X. Mi, and M. W. Khan, "Fractional order sliding mode based direct power control of grid-connected DFIG," *IEEE Trans. on Power Systems*, vol. 33, no. 3, pp. 3087–3096, 2018.

[17] D. Sun, X. Wang, H. Nian, and Z. Q. Zhu, "A sliding-mode direct power control strategy for DFIG under both balanced and unbalanced grid conditions using extended active power," *IEEE Trans. on Power Electronics*, vol. 33, no. 2, pp. 1313–1322, 2018.
[18] C. A. Evangelista, A. Pisano, P. Puleston, and E. Usai, "Receding horizon adaptive second-order sliding mode control for doubly-fed induction generator based wind turbine," *IEEE Trans. on Control Systems Technology*, vol. 25, no. 1, pp. 73–84, 2017.
[19] A. Djoudi, S. Bacha, H. Chekireb, H. Iman-Eini, and C. Boudinet, "Adaptive sensorless SM-DPC of DFIG-based WECS under disturbed grid: Study and experimental results," *IEEE Trans. on Sustainable Energy*, vol. 9, no. 2, pp. 570–581, 2018.
[20] I. Villanueva, A. Rosales, P. Ponce, and A. Molina, "Grid-voltage-oriented sliding mode control for DFIG under balanced and unbalanced grid faults," *IEEE Trans. on Sustainable Energy*, vol. 9, no. 3, pp. 1090–1098, 2018.
[21] D. Novotny and J. H. Wouterse, "Induction machine transfer functions and dynamic response by means of complex time variables," *IEEE Trans. on Power Apparatus and Systems*, vol. 95, no. 4, pp. 1325–1335, 1976.
[22] A. Dòria-Cerezo, M. Bodson, C. Batlle, and R. Ortega, "Study of the stability of a direct stator current controller for a doubly-fed induction machine using the complex Hurwitz test," *IEEE Trans. on Control Systems Technology*, vol. 21, no. 6, pp. 2323–2331, 2013.
[23] H. J. Baesmat and M. Bodson, "Pole placement control for doubly-fed induction generators using compact representations in complex variables," *IEEE Trans. on Energy Conversion*, vol. 34, no. 2, pp. 750–760, 2019.
[24] M. Bodson, "Speed control for doubly fed induction motors with and without current feedback," *IEEE Trans. on Control Systems Technology*, vol. 28, no. 3, pp. 898–907, 2020.
[25] A. Dòria-Cerezo, J. M. Olm, D. Biel, and E. Fossas, "Sliding modes of complex-valued nonlinear systems," *IEEE Trans. on Automatic Control*, vol. 66, no. 7, pp. 3355–3362, 2021.
[26] A. Dòria-Cerezo, J. M. Olm, V. Repecho, and D. Biel, "Complex-valued sliding mode control of an induction motor," in *Proc. IFAC World Congress*, 2020.
[27] D. W. Novotny and T. A. Lipo, *Vector Control and Dynamics of AC Drives*. London, U.K.: Oxford Univ. Press, 1996.
[28] A. Dòria-Cerezo, "Comments on "control and performance of a doubly-fed induction machine intended for a flywheel energy storage system"," *IEEE Trans. on Power Electronics*, vol. 28, no. 1, pp. 605–606, 2013.

Arnau Dòria-Cerezo was born in Barcelona, Spain, in 1974. He received the undergraduate degree in electromechanical engineering from the Universitat Politècnica de Catalunya (UPC), Barcelona, Spain, in 2001, the D.E.A. degree in industrial automation from the Institut National des Sciences Appliquées de Lyon, Villeurbanne, France, in 2001, and the Ph.D. degree in advanced automation and robotics from UPC in 2006.

He is currently an Associate Professor with the Department of Electrical Engineering, UPC, and carries on his research activities with the Advanced Control of Energy Systems Group, Institute of Industrial and Control Engineering, UPC. In 2010, he was a Visitor at the Technische Universiteit Delft, Delft, The Netherlands. From 2003 to 2004, he was a Control Training Site-Research Fellow with the Laboratoire des Signaux et Systèmes, Supélec, France. He was an Associate Editor for *Control Engineering Practice* from 2017 to 2022. His research interests include modeling and control of electrical systems and automotive applications.

Md Abid Hossain (M'18) received the B.Sc. degree in electrical and electronics engineering from Bangladesh University of Engineering and Technology, Dhaka, Bangladesh, in 2013 and the M.S. and Ph.D. in electrical engineering from the University of Utah, UT, USA in 2017 and 2022.

He is working as an Associate System Engineer in Nexteer Automotive. His previous experience includes working as a lecturer in the Department of Electrical and Electronics Engineering of Bangladesh University of Business and Technology.

Marc Bodson (F'06) received the Ingénieur Civil Mécanicien et Electricien degree from the Université Libre de Bruxelles, Brussels, Belgium, in 1980, two M.S. degrees, one in electrical engineering and computer science and one in aeronautics and astronautics, from the Massachusetts Institute of Technology, Cambridge, MA, USA, in 1982, and the Ph.D. degree in electrical engineering and computer science from the University of California at Berkeley, Berkeley, CA, USA, in 1986.

He is currently a Professor of Electrical and Computer Engineering with the University of Utah, Salt Lake City, UT, USA. He was Chair of the Department of Electrical and Computer Engineering from 2003 to 2009. He was the Editor-in-Chief for the *IEEE Transactions on Control Systems Technology* from 2000 to 2003. He was elected Associate Fellow of the AIAA in 2013. His activities are described in further detail at www.ece.utah.edu/∼bodson